



Bottom-Up Determination of Air-Sea Momentum Exchange Under a Major Tropical Cyclone

Ewa Jarosz, *et al.*
Science **315**, 1707 (2007);
DOI: 10.1126/science.1136466

The following resources related to this article are available online at www.sciencemag.org (this information is current as of March 28, 2007):

Updated information and services, including high-resolution figures, can be found in the online version of this article at:

<http://www.sciencemag.org/cgi/content/full/315/5819/1707>

Supporting Online Material can be found at:

<http://www.sciencemag.org/cgi/content/full/315/5819/1707/DC1>

This article **cites 3 articles**, 1 of which can be accessed for free:

<http://www.sciencemag.org/cgi/content/full/315/5819/1707#otherarticles>

This article appears in the following **subject collections**:

Oceanography

<http://www.sciencemag.org/cgi/collection/oceans>

Information about obtaining **reprints** of this article or about obtaining **permission to reproduce this article** in whole or in part can be found at:

<http://www.sciencemag.org/about/permissions.dtl>

5. R. J. Stern, *Geology* **33**, 557 (2005).
6. T. M. Kusky, J.-H. Li, R. D. Tucker, *Science* **292**, 1142 (2001).
7. M. Zhai, G. Zhao, Q. Zhang, *Science* **295**, 923a (2002).
8. T. M. Kusky, Ed., *Precambrian Ophiolites and Related Rocks* (Elsevier, Amsterdam, 2004).
9. M. J. de Wit, in *Developments in Precambrian Geology*, vol. 13, T. M. Kusky, Ed. (Elsevier, London, 2004), pp. 599–614.
10. A. P. Nutman, *Greenland Geol. Surv. Bulletin* 154 (1986).
11. M. T. Rosing, N. M. Rose, D. Bridgwater, H. S. Thomsen, *Geology* **24**, 43 (1996).
12. T. Komiya *et al.*, *J. Geol.* **107**, 515 (1999).
13. J. S. Myers, *Precambrian Res.* **105**, 129 (2001).
14. A. P. Nutman, V. C. Bennett, C. R. L. Friend, M. T. Rosing, *Chem. Geol.* **141**, 271 (1997).
15. M. T. Rosing, *Science* **283**, 674 (1999).
16. M. Boyet *et al.*, *Earth Planet. Sci. Lett.* **214**, 427 (2003).
17. A. Polat, A. W. Hofmann, M. T. Rosing, *Chem. Geol.* **184**, 231 (2002).
18. A. P. Nutman, V. R. McGregor, C. R. L. Friend, V. C. Bennett, P. D. Kinny, *Precambrian Res.* **78**, 1 (1996).
19. A. Polat, A. W. Hofmann, *Precambrian Res.* **126**, 197 (2003).
20. Y. Dilek, M. J. F. Flower, *Geol. Soc. London Spec. Publ.* **218**, 43 (2003).
21. A. J. Crawford, Ed., *Boninites* (Unwin Hyman, London, 1989).
22. R. B. Pedersen, H. Furnes, *J. Geodyn.* **13**, 183 (1991).
23. K. Muehlenbachs, *Chem. Geol.* **145**, 263 (1998).
24. D. S. Stakes, H. P. Taylor Jr., *J. Geophys. Res.* **97**, 7043 (1992).
25. C. Holmden, K. Muehlenbachs, *Science* **259**, 1733 (1993).
26. J. L. R. Touret, *Precambrian Res.* **126**, 219 (2003).
27. Comments by Y. Dilek, B. Robins, N. McLoughlin, and two anonymous reviewers improved the manuscript. Financial support was provided by the Norwegian Research Council, the Geological Museum of Copenhagen, the GFZ-Potsdam, the Agouron foundation, and the National Sciences and Engineering Research Council of Canada. This is AEON contribution no. 31.

Supporting Online Material

www.sciencemag.org/cgi/content/full/315/5819/1704/DC1
SOM Text
Figs. S1 to S4
Table S1
References

21 December 2006; accepted 7 February 2007
10.1126/science.1139170

Bottom-Up Determination of Air-Sea Momentum Exchange Under a Major Tropical Cyclone

Ewa Jarosz,* Douglas A. Mitchell,† David W. Wang, William J. Teague

As a result of increasing frequency and intensity of tropical cyclones, an accurate forecasting of cyclone evolution and ocean response is becoming even more important to reduce threats to lives and property in coastal regions. To improve predictions, accurate evaluation of the air-sea momentum exchange is required. Using current observations recorded during a major tropical cyclone, we have estimated this momentum transfer from the ocean side of the air-sea interface, and we discuss it in terms of the drag coefficient. For winds between 20 and 48 meters per second, this coefficient initially increases and peaks at winds of about 32 meters per second before decreasing.

The air-sea momentum exchange under a tropical cyclone determines the oceanic response to its winds. An accurate estimation of the exchange hence is required for correctly forecasting storm track and intensity, as well as for accurately predicting storm surges, ocean currents, and waves, and for making hurricane risk assessments, particularly because the frequency and intensity of tropical cyclones are reportedly increasing (1). Conventional methods of determining the air-sea momentum transfer are from the atmospheric side of the interface and are based on measurements of wind profiles near the ocean surface or of wind turbulence (2). These methods, however, cannot work reliably for the extreme high-wind conditions of a major tropical cyclone, because wind measurements near the ocean interface are inevitably contaminated from intense breaking-wave activities and sea spray (3).

Most available field measurements of surface stress are for wind speeds ranging from 4 to

20 m s⁻¹. The techniques employed estimate the interface momentum exchange as a wind stress, τ_s , given by

$$\tau_s = \rho_{\text{air}} C_D |\mathbf{W}|^2 \quad (1)$$

where ρ_{air} is the air density, C_D is the drag coefficient, and $|\mathbf{W}|$ is the velocity magnitude of the wind at a reference height (usually 10 m).

In open ocean conditions, as the wind becomes stronger the range of surface waves, which travel at slower speeds than the wind, widens. Accordingly, C_D increases as wind speed increases (3). This pattern of variability in C_D is commonly used in wave, surge, and circulation numerical models, which incorporate a monotonic increase of the drag coefficient with wind speed even under extreme wind conditions. Such an assumption may result in an overestimation of the air-sea momentum transfer and lead to unrealistic model predictions or, perhaps even worse, model tuning using bad physical justifications.

Recently, limited meteorological observations, theory, and experiments (3–8) suggest a reduction in the drag coefficient at high wind speeds, generally greater than 30 m s⁻¹. All these efforts to evaluate the air-sea momentum exchange have been made through meteorological measurements, or theories and models developed

for the atmospheric boundary layer (“top-down” determination). Estimation of this exchange can also be done from the other side of the interface with full water-column ocean current observations. This method directly determines the stress at the interface based on ocean currents and provides a very reliable and accurate direct determination of the air-sea momentum transfer under high winds (3). However, this type of “bottom-up” determination imposes the almost impossible requirements of deploying instruments in the ocean directly under the highly unpredictable path of a major tropical cyclone and then having the instruments survive the enormous forces generated by the cyclone.

On 15 September 2004, the center of Hurricane Ivan (at category 4 strength) passed directly over six current and wave/tide gauge moorings on the outer continental shelf in the northeastern Gulf of Mexico (9–12) (Fig. 1). The instrumentation survived and measured nearly full ocean current velocity profiles directly under the cyclone. The resulting data set allows direct “bottom-up” determination of the air-sea momentum exchange under extreme wind conditions.

Extreme winds of a tropical cyclone elicit a four-stage response when passing over ocean waters (9, 13). The first three stages make up the “forced stage” response, whereas the fourth stage is the “relaxation stage.” Over the open ocean, the forced stage response is primarily baroclinic (depth-dependent), with a weak barotropic (depth-independent) response consisting of a trough in sea surface height and an associated geostrophic current that are set up almost instantly (13). Over the continental shelf, however, the forced response is quite different (9). It consists of a strong barotropic component that is not geostrophically balanced and a much weaker baroclinic response. Thus, the directly forced response on the continental shelf should be well described to the first order by the linear time-dependent depth-integrated horizontal momentum equations. Scaling analysis of current velocity measurements recorded in the northeastern Gulf of Mexico (Fig. 1) under Hurricane Ivan supports this assumption, especially for the along-

Naval Research Laboratory, Stennis Space Center, MS 39529–5004, USA.

*To whom correspondence should be addressed. E-mail: ewa.jarosz@nrlssc.navy.mil

†Present address: Exxon Mobil Upstream Research Company, Houston, TX 77027–6019, USA.

Fig. 1. Regional map and instrument locations. Bathymetry (in meters) is shown for the north-eastern Gulf of Mexico. Acoustic Doppler current profiler (ADCP) moorings are denoted by black dots (M1 to M6). The yellow triangle is Buoy 42040, National Data Buoy Center. Hurricane Ivan's path is indicated by the dashed red line. Two inserts in the expanded map are a colored infrared image of Hurricane Ivan taken by the National Oceanic and Atmospheric Administration's Geostationary Operational Environmental Satellite-12 satellite (lower right) and a Barny mooring containing the ADCP current meter (upper right).

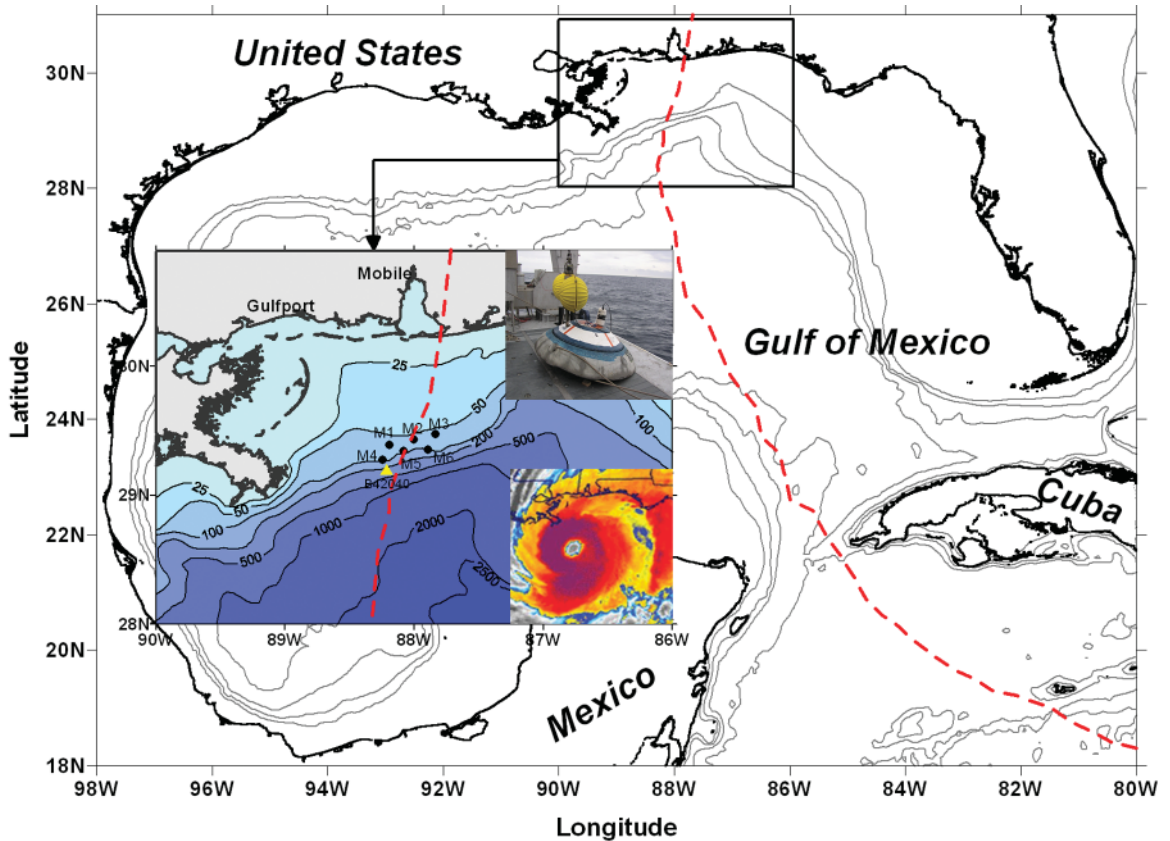
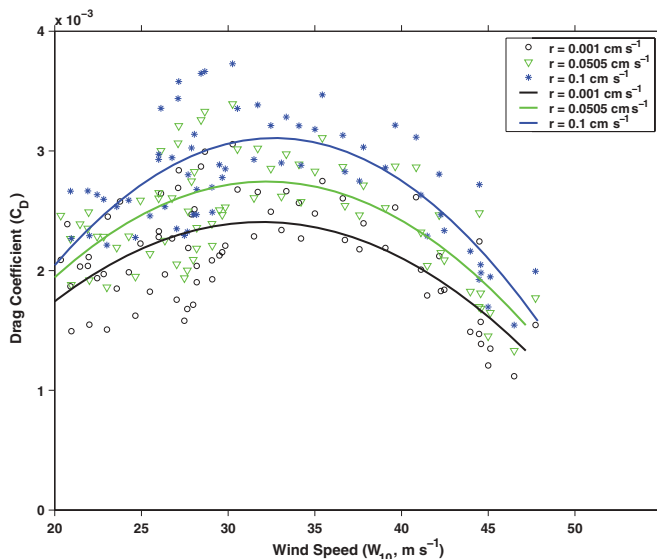


Fig. 2. Drag coefficient for several resistance coefficients. C_D is shown as a function of the wind speed at 10 m (W_{10}) for several different resistance coefficients r (open black circles – $r = 0.001 \text{ cm s}^{-1}$; green triangles – $r = 0.0505 \text{ cm s}^{-1}$; blue asterisks – $r = 0.1 \text{ cm s}^{-1}$). The solid lines represent quadratic curves fitted to the evaluated C_D separately for each r .



shelf momentum [more discussion concerning the along-shelf momentum balance is in (14)] given by

$$\frac{\partial U}{\partial t} - fV = \frac{\tau_{sx}}{\rho H} - \frac{rU}{H} \quad (2)$$

where ρ is a reference density (1025 kg m^{-3}), f is the Coriolis parameter ($0.71 \times 10^{-4} \text{ s}^{-1}$), U and V are the depth-integrated along-shelf and cross-shelf velocity components, H is the water depth, r is a constant resistance coefficient at

the sea floor, and τ_{sx} is the along-shelf wind stress.

The simplified dynamics given by Eq. 2 may not hold under all conditions. For instance, in this case, the momentum balance breaks down once the eye of the storm has passed over the moorings and the wind vectors rapidly rotate 180° . When this happens, the water column cannot respond and change direction as rapidly as the wind, and these dynamics no longer hold. Additionally, the momentum balance may not hold for a rapidly moving tropical cyclone or for a cyclone with an

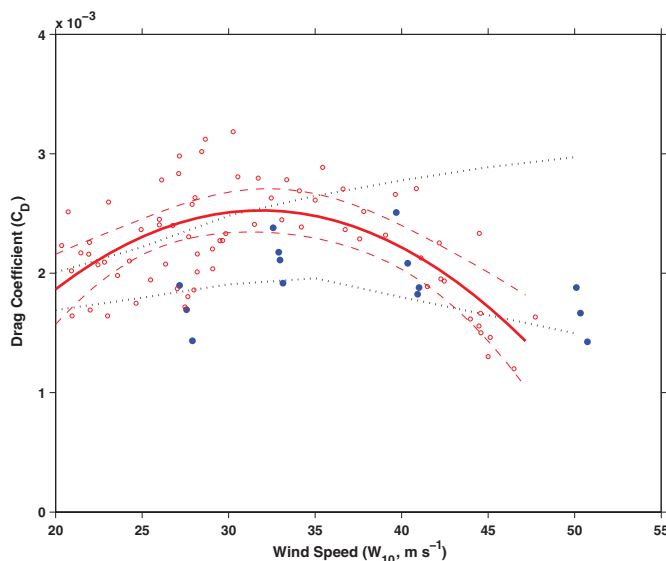
erratic path for similar reasons. However, many cyclones move slowly and steadily enough over the shelf for such an approximation to hold.

The air-sea momentum transfer, expressed in terms of τ_{sx} , is estimated from Eq. 2 using our ocean current observations. In atmospheric studies, this exchange is commonly discussed in terms of the drag coefficient (C_D). Wind stress (τ_{sx}) can be also defined as $\tau_{sx} = \rho_{\text{air}} C_D |\mathbf{W}| W_x$, where W_x is the along-shelf wind velocity component. Thus, for comparison with other studies, we can determine C_D by inserting the formula for τ_{sx} into Eq. 2.

$$C_D = \frac{\rho H}{\rho_{\text{air}} |\mathbf{W}| W_x} \left(\frac{\partial U}{\partial t} - fV + \frac{rU}{H} \right) \quad (3)$$

Results produced from evaluation of Eq. 3 are shown in Figs. 2 and 3. The drag coefficient was derived for several different values of the resistance coefficient (r) ranging between 0.001 cm s^{-1} and 0.1 cm s^{-1} . These values of r are similar to those used in other studies investigating shelf currents (15–18). Figure 2 displays estimates of C_D for minimum (0.001 cm s^{-1}), mean (0.0505 cm s^{-1}), and maximum (0.1 cm s^{-1}) values of r used in Eq. 3, whereas Fig. 3 shows results for $r = 0.02 \text{ cm s}^{-1}$, that is, the resistance coefficient that was determined from observations for the northeastern shelf of the Gulf of Mexico (15). The results, especially for the wind

Fig. 3. Drag coefficient as a function of wind speed. C_D is shown for an observation-based resistance coefficient, $r = 0.02 \text{ cm s}^{-1}$. The red open circles are the evaluated C_D from the current and wind observations, the solid red line is a fitted quadratic curve to the C_D estimates, and the red dashed lines are the 95% confidence limits for this quadratic curve. The black dotted lines represent the window for C_D reported in (6), whereas the blue dots represent C_D reported in (4).



speeds below 30 m s^{-1} , are somewhat noisy as a result of measurement uncertainty and the need to calculate a velocity derivative, which tends to enhance noise. However, they consistently show a decreasing trend of C_D for wind speeds greater than 32 m s^{-1} , the lower threshold for a category 1 hurricane on the Saffir-Simpson Scale. It is also apparent that the C_D values are weakly dependent on the choice of the resistance coefficient and are larger for increasing values of r . The drag coefficient estimates evaluated for $r = 0.1 \text{ cm s}^{-1}$ are, on average, 20% greater than those calculated for $r = 0.001 \text{ cm s}^{-1}$ from Eq. 3.

To produce the best representation of C_D for each r , a second-order curve (a function of the wind speed) was fitted by a least-squares technique to all estimated values of C_D . The curves are displayed in Figs. 2 and 3. Additionally, the 95% confidence limits for the fitted curve are shown in Fig. 3. The pattern of the relationship between C_D and the wind speed is robust, but the curve coefficients are determined by the value chosen for r in Eq. 3. However, all curves clearly show an initial increase of the drag coefficient and monotonic decrease as found by recent studies (3–8) after reaching a maximum value at $\sim 32 \text{ m s}^{-1}$. Some of these studies (3, 19) imply that the decreasing drag at high winds seems to be related to the spray, foam, and bubbles from breaking waves that reduce the drag and allow the hurricane to slip over the sea.

With the nearly full water-column ocean current measurements, the only unknown term left in the simplified equation of motion is the wind stress. Thus, the behavior of the drag coefficient (C_D) can easily be estimated for a range of strong winds. Despite the fact that the drag coefficient is evaluated differently here, estimates of C_D determined “bottom-up” reasonably replicate the values determined “top-down” in recent studies (3–7). Results from our research show that C_D peaks at a wind speed near 32 m s^{-1} and

then steadily decreases as the wind speed continues to rise. Our values for C_D are in a range of C_D values found using meteorological observations (4) for wind speeds greater than 32 m s^{-1} but are higher for lower wind speeds. These differences may be attributed to uncertainties in the wind measurements and the applicability of the simplified ocean dynamics at the lower wind speeds.

References and Notes

1. K. Emanuel, *Nature* **436**, 686 (2005).
2. S. E. Larsen *et al.*, in *Wind Stress Over the Ocean*, I. S. F. Jones, Y. Toba, Eds. (Cambridge Univ. Press, New York, 2001), chap. 7.
3. M. A. Donelan *et al.*, *Geophys. Res. Lett.* **31**, L18306 10.1029/2004GL019460 (2004).

4. M. D. Powell, P. J. Vickery, T. A. Reinhold, *Nature* **422**, 279 (2003).
5. E. D. Fernandez *et al.*, *J. Geophys. Res.* **111**, C08013 10.1029/2005JG003048 (2006).
6. I. J. Moon, I. Ginis, T. Hara, *J. Atmos. Sci.* **61**, 2334 (2004).
7. J. A. T. Bye, A. D. Jenkins, *J. Geophys. Res.* **111**, C03024 10.1029/2005JG003114 (2006).
8. K. Emanuel, *J. Atmos. Sci.* **60**, 1420 (2003).
9. D. A. Mitchell, W. J. Teague, E. Jarosz, D. W. Wang, *Geophys. Res. Lett.* **32**, L11610 10.1029/2005GL023014 (2005).
10. D. W. Wang, D. A. Mitchell, W. J. Teague, E. Jarosz, M. S. Hulbert, *Science* **309**, 896 (2005).
11. W. J. Teague, E. Jarosz, D. W. Wang, D. A. Mitchell, *J. Phys. Oceanogr.*, in press.
12. W. J. Teague, E. Jarosz, M. R. Carnes, D. A. Mitchell, P. J. Hogan, *Cont. Shelf Res.* **26**, 2559 (2006).
13. J. F. Price, T. B. Sanford, G. Z. Forristall, *J. Phys. Oceanogr.* **24**, 233 (1994).
14. Materials and methods are available as supporting material on Science Online.
15. G. T. Mitchum, W. Sturges, *J. Phys. Oceanogr.* **12**, 1310 (1982).
16. S. T. Lentz, *J. Phys. Oceanogr.* **24**, 2461 (1994).
17. S. J. Lentz, *J. Phys. Oceanogr.* **31**, 2749 (2001).
18. J. M. Pringle, *J. Phys. Oceanogr.* **32**, 3101 (2002).
19. E. L. Andreas, *J. Phys. Oceanogr.* **34**, 1429 (2004).
20. We thank M. S. Hulbert, A. J. Quaid, and W. A. Goode for mooring support. We also thank the crews of the research vessels Seward Johnson I and II. This work was supported by the Office of Naval Research as a part of the Naval Research Laboratory’s basic research project “Slope to Shelf Energetics and Exchange Dynamics (SEED)” under program element 0601153N, through the Minerals Management Service Environmental Studies Program Technology, and by the Minerals Management Service Technology Assessment and Research Program on Hurricane Ivan.

Supporting Online Material

www.sciencemag.org/cgi/content/full/315/5819/1707/DC1
SOM Text

Fig. S1
References

18 October 2006; accepted 14 February 2007
10.1126/science.1136466

CRISPR Provides Acquired Resistance Against Viruses in Prokaryotes

Rodolphe Barrangou,¹ Christophe Fremaux,² H el ene Deveau,³ Melissa Richards,¹ Patrick Boyaval,² Sylvain Moineau,³ Dennis A. Romero,¹ Philippe Horvath^{2*}

Clustered regularly interspaced short palindromic repeats (CRISPR) are a distinctive feature of the genomes of most Bacteria and Archaea and are thought to be involved in resistance to bacteriophages. We found that, after viral challenge, bacteria integrated new spacers derived from phage genomic sequences. Removal or addition of particular spacers modified the phage-resistance phenotype of the cell. Thus, CRISPR, together with associated *cas* genes, provided resistance against phages, and resistance specificity is determined by spacer-phage sequence similarity.

Bacteriophages are arguably the most abundant biological entity on the planet (1). Their ubiquitous distribution and abundance have an important impact on microbial ecology and the evolution of bacterial genomes (2). Consequently, bacteria have developed a variety of natural defense mechanisms that target diverse steps of the phage life cycle, notably blocking adsorption, preventing DNA

injection, restricting the incoming DNA, and abortive infection systems. These antiviral barriers can also be engineered and manipulated to better control phage populations (2, 3).

Numerous bacteria have been selected by humans and used extensively for fermentation and biotechnology processes. Unfortunately, domesticated bacteria used in industrial applications are often susceptible to phage attack, including